Sensory diversity and precise adaptation enable independent bet-hedging strategies for multiple signals at the same time

Jeremy Philippe Moore†, Keita Kamino†, Rafaela Kottou, Thomas Shimizu, Thierry Emonet*

*For correspondence: thierry.emonet@yale.edu

†These authors contributed equally to this work

Abstract:

While navigating their environments, cells encounter many different signals at once. In the face of uncertain conditions, diversifying the sensitivity to different signals across the population can be useful. Previous studies established that one of the simplest sensory systems, the chemotaxis network of *Escherichia coli*, can switch between a high diversity bet-hedging strategy, and a low diversity tracking strategy for a ligand as that ligand becomes prevalent. Here, we combine mathematical modeling and single-cell experiments to show that populations of chemotactic bacteria make this transition for each ligand independently. That is, transitioning to tracking one ligand does not compromise the population's ability to hedge its bets across other future ligands. Remarkably, we found that this independence holds even if those ligands compete for receptor binding sites with the background ligand being tracked. The independence of this transition between two diversity regimes is explained by a simple allosteric model of chemoreceptor clusters with negative integral feedback, which accurately predicts the observed diversity in sensitivity under various background stimulus conditions. Our mathematical analysis shows that similar transitions from bet-hedging to tracking also arise in feed-forward network architectures capable of precise adaptation, suggesting that environment-dependent modulation of diversity may occur in many cell types.

Introduction:

In their environments, organisms must sense and respond to some signals embedded in a complex backdrop of other stimuli. To solve this problem, sensory systems have evolved to integrate signals and make decisions. In fly olfaction for examples, relatively few olfactory receptors (~50) are used to encode and identify an enormous range of stimuli to drive a highly olfaction-dependent lifestyle (Hallem and Carlson, 2006; Kadakia and Emonet, 2019; Pfister et al., 2020; Qin et al., 2019). Similarly, many bacteria use a small set (~3) of quorum-sensing receptors to drive the switch between biofilm and planktonic lifestyles as the ratio of signals secreted by self and other bacteria changes (Hurley and Bassler, 2017; Narla et al., 2021). In both these cases, a downstream network – neural in the fly case and transcriptional in the quorum-sensing case – is used to parse the integrated signals and prevent signal cross-talk.

An extreme example of signal integration is the chemosensory network of *Escherichia coli*. In this system, chemoreceptors are organized into highly cooperative receptor-kinase complexes (Burt et al., 2020). These complexes phosphorylate a single response regulator which controls

flagellar rotation. Addition and removal of methyl groups from the receptors by methyl-transferase CheR and methylesterase CheB allow the kinase activity to adapt to background stimuli, and respond sensitively over multiple decades of ligand concentration (Parkinson et al., 2015; Sourjik and Berg, 2002, 2004). Given the simplicity of this signaling system, it is unclear how single bacteria navigate a realistic environment with many overlapping stimuli. Although *E. coli* express five receptor species, all receptors belong to the same allosteric clusters, and modulate the activity of the same kinase. As such, how can cells navigate a complex chemical landscape with many signals present at once?

One hypothesis is that individual cells are poor navigators on their own. However, isogenic cell populations generate individuals with diverse sensitivity to different stimuli, allowing them to hedge their bets against changes in available attractant gradients and effectively explore complex environments (Frankel et al., 2014; Karin and Alon, 2021; Salek et al., 2019). Recent developments in single-cell fluorescence resonance energy transfer (FRET) have allowed this diversity to be probed at the signal-transduction level (Colin et al., 2017; Keegstra et al., 2017). These studies revealed diverse sensitivities to various attractants, and confirmed cell-to-cell variability in kinase activity fluctuation (Korobkova et al., 2004; Park et al., 2010).

Recently, using single-cell FRET, we discovered that the degree of cell-to-cell variation in sensitivity to an attractant depends on its background concentration. When the background concentration of the attractant alpha-methyl-aspartate (meAsp) is low, sensitivity to meAsp varies greatly from cell to cell. However, after the cells have adapted to a sufficiently high background of meAsp, the degree of variation in sensitivity within the clonal population is strongly attenuated (Kamino et al., 2020). This “diversity tuning” occurs without changes in gene expression and was hypothesized to play a role in a population’s ability to switch between different navigational strategies on the fly while exploring the environment. When attractant concentration is low, populations can hedge their bets by diversifying their sensitivities to stimuli. However, after detecting a sufficiently strong signal, the population shifts to a tracking strategy where each individual is tuned to the gradient.

What remains untested is whether and how diversity tuning applies to the more ecologically relevant scenarios involving multiple ligand stimuli. Does adding one stimulus to the environment affect the ability of the population to modulate the sensitivity distribution for other stimuli? Are there different effects when background ligands compete with the foreground for binding sites and when they do not?

Here, we used microfluidics and single-cell FRET to determine how sensitivities for several ligands are distributed in different stimulus backgrounds. For ligands that bind to different receptors, we find that the sensitivity distributions can be tuned independently even if those receptors are allosterically coupled. Thus, a population can take advantage of sensory bet-hedging even in the presence of other signals. Remarkably, even for ligands that compete for binding sites on the same receptor, transitioning to the low-diversity regime for one ligand does not reduce the diversity for other signals. Using a quantitative model of chemoreceptors, we predict the signal concentration where the switch occurs, which we verify using experiments. Last, we examine several mathematical models of adaptive incoherent feed-forward loops and show that this general

class of signaling networks is also able to display background-dependent sensory diversity when this diversity arises at specific points in the network.

Results:

Measuring single-cell responses:

We set out to measure the distribution of sensitivity for one ligand species in the presence of different background ligand mixtures. We quantified sensitivity by the $K_{1/2}$, which we defined as the ligand concentration where kinase activity reached half of its steady-state value. For simplicity, we focused on ligands that bind the two highest-expressed receptors in *E. coli*: Tar and Tsr (Figure 1A).

For a given combination of foreground and background stimulus, we measured the $K_{1/2}$ distribution using an extension of previous methods (Kamino et al., 2020). We developed a microfluidic device with seven input channels (Figure 1B; Figure S1A-D) which allows us to deliver solutions to cells immobilized in the device. The time to switch stimuli is ~100ms, enabling quantification of kinase activity responses to small stimuli without the confounding effects of adaptation. This new device allows us to measure the $K_{1/2}$ CDF for one combination of foreground and background stimulus in a single experiment, unlike previous methods where multiple experiments were required.

After adaptation to the background stimulus, five levels of the foreground were presented in series, seven times (light grey curves in Figure 1CD). Each stimulus lasted for 5 seconds with 30 seconds between measurements to allow adaptation back to steady state. Between measurements the cells were not imaged to reduce photobleaching. For a given stimulus level, the seven individual responses were averaged (black curves in Figure 1CD). We defined the response amplitude as the average post-stimulus activity minus the average pre-stimulus activity, normalized by the pre-stimulus activity. Zero-activity was defined as the kinase activity immediately after a saturating stimulus.

The distribution of $K_{1/2}$ can be extracted from the distribution of response amplitudes for different stimulus concentrations (Kamino et al., 2020). As described previously, for a population of bacteria, the value of the cumulative distribution function (CDF) of the $K_{1/2}$ is given by the fraction of responses greater than half the maximal response (Figure S1E,F). This relationship is valid when the response distribution is stationary, which is the case with our experiment (Figure S2A). We fit a log-normal CDF to the measured $K_{1/2}$ CDF to extract the mean and standard deviation of the $\log(K_{1/2})$ (Figure 2AB; Figure S2B,C). We then verified that as in previous work, the $K_{1/2}$ distribution for meAsp was broad when the background [meAsp] was 0, and narrow after adaptation to $100\mu M$ meAsp (Figure 2B).

Our method allowed us to make detailed single-cell measurements, and compare cell-to-cell variability in a variety of background stimulus conditions. Responses to the same signal vary greatly both within cells across the seven identical stimuli, and from cell to cell (Figure 1C, D).

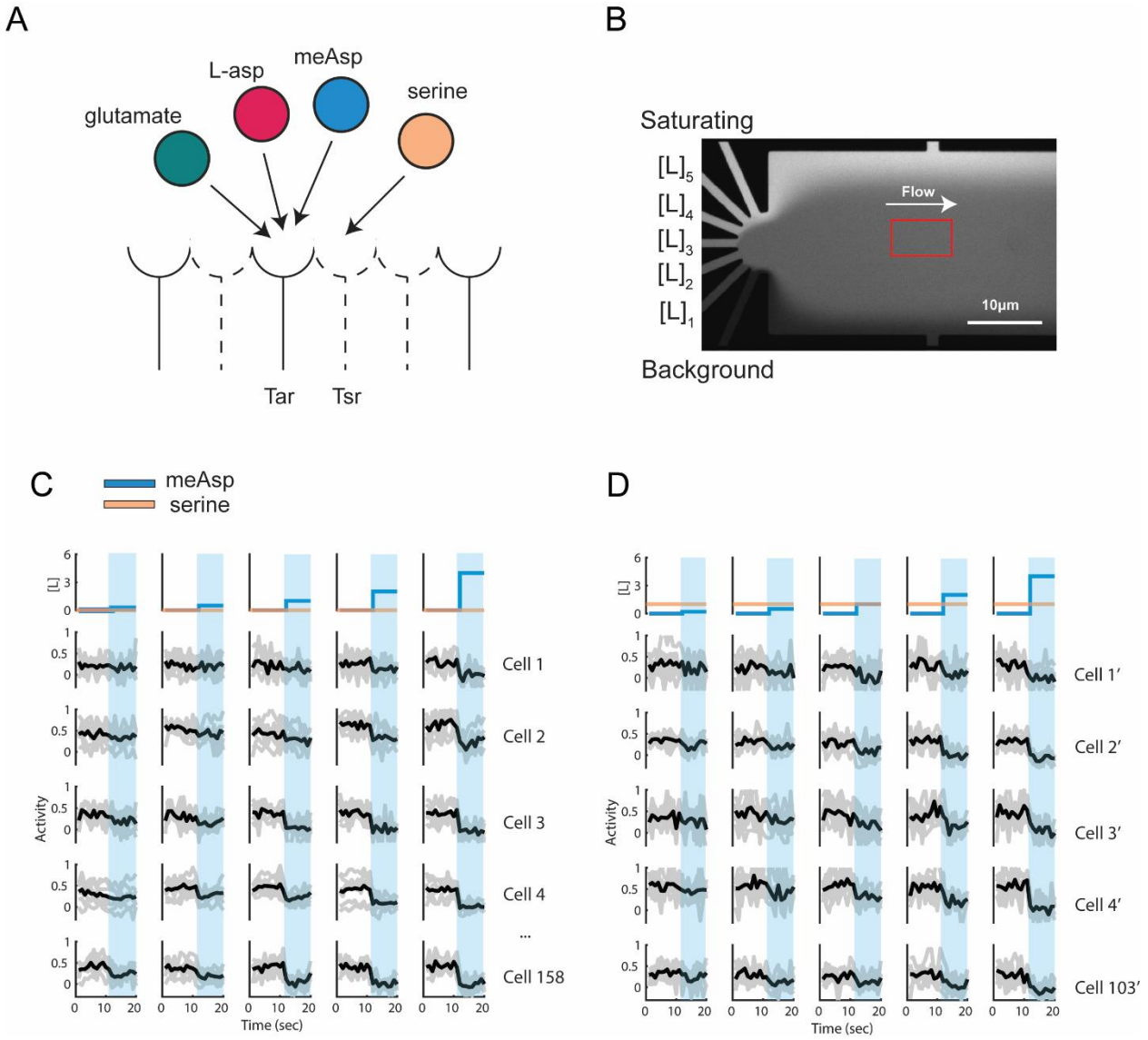

Figure 1. Measuring chemosensory response variation with various combinations of background and foreground ligands. A) *E. coli* are able to sense various ligands. We measured responses to 3 ligands that bind the Tar receptor, and one that binds Tsr after adaptation to various mixtures of background ligands. **B)** Measurements were performed in a microfluidic device capable of exchanging media in the field-of-view in ~100ms. The device has seven inlets: one contains only the background stimulus, one a saturating stimulus to determine maximal response amplitude, and five different test stimulus levels. **C)** Single cell responses to five different meAsp concentrations with no background ligands present. For each stimulus level, seven responses were measured per cell. Individual responses are in gray, with the within-cell averages shown in black. **D)** Responses to the same five meAsp concentrations in the presence of a 1 uM serine background.

Some cells are more random than others in their responses to the same signal presented multiple time. Some cells respond very sensitively to small stimuli, while others barely respond.

Independent diversity tuning for ligands that bind different receptors

Using our new microfluidic device to measure the $K_{1/2}$ distribution, we first investigated how adaptation to a ligand that binds one receptor affects the $K_{1/2}$ distribution for ligands that bind a different receptor (Figure 2A). It was previously shown that at the population-average level, serine, which binds Tsr with high affinity ($K_{1/2} \approx 10^{-1}\mu M$) and Tar with low affinity ($K_{1/2} \approx 10^{1}\mu M$), does not significantly affect the $K_{1/2}$ of MeAsp, which primarily binds Tar (Neumann et al., 2010; Yang et al., 2015). We were interested in whether this preservation of mean sensitivity was accompanied by a preservation of the standard deviation in $K_{1/2}$.

We measured the CDF of $K_{1/2}$ for meAsp and serine in four background conditions: zero-background (plain motility medium), $100\mu M$ meAsp, $1\mu M$ serine, and a mixture of $100\mu M$ meAsp and $1\mu M$ serine. These concentrations were chosen because they are sufficient to collapse the meAsp and serine $K_{1/2}$ distributions upon adaptation to a background of the same signals (Kamino et al., 2020). A lognormal CDF was fit to each dataset, from which the mean and coefficient of variation (CV) were calculated from the fitted log-normal parameters. Data collected from at least two biological replicates were included in each analysis to increase the number of cells per data point.

As in our previous studies (Kamino et al., 2020), adaptation to $100\mu M$ MeAsp led to a collapse in the $K_{1/2}$ distribution for MeAsp, with a drastic decrease in CV (Figures 2B; Figure S3). However, adaptation to $1\mu M$ serine had no detectable effect on the $K_{1/2}$ distribution for MeAsp (Figure 2C; Figure S3). Similarly, while adaptation to $1\mu M$ serine background collapses the serine $K_{1/2}$ distribution (Figures 2D and S3), adaptation to $100\mu M$ meAsp did not significantly affect the serine $K_{1/2}$ distribution (Figures 2E; Figure S3).

This experiment suggests that in addition to maintaining the same mean sensitivity for meAsp (serine) in the presence of serine (meAsp), the bacterial populations also maintain variability in sensitivity. As such, even though receptor clusters inside individual cells can be comprised of a mixture of receptor types that act cooperatively (Frank et al., 2016; Lan et al., 2011; Piñas et al., 2016), populations of *E. coli* can independently tune the $K_{1/2}$ distributions for ligands that bind different receptors.

Receptor-ligand affinity does not affect the degree of sensory diversity

Next, we decided to measure how ligands that compete for binding on the same receptor affect each other's $K_{1/2}$ distributions. As ligands we used meAsp, L-Asp, and glutamate (Figure 3A), which are known to primarily bind Tar and not Tsr (Yang et al., 2015). We first measured the

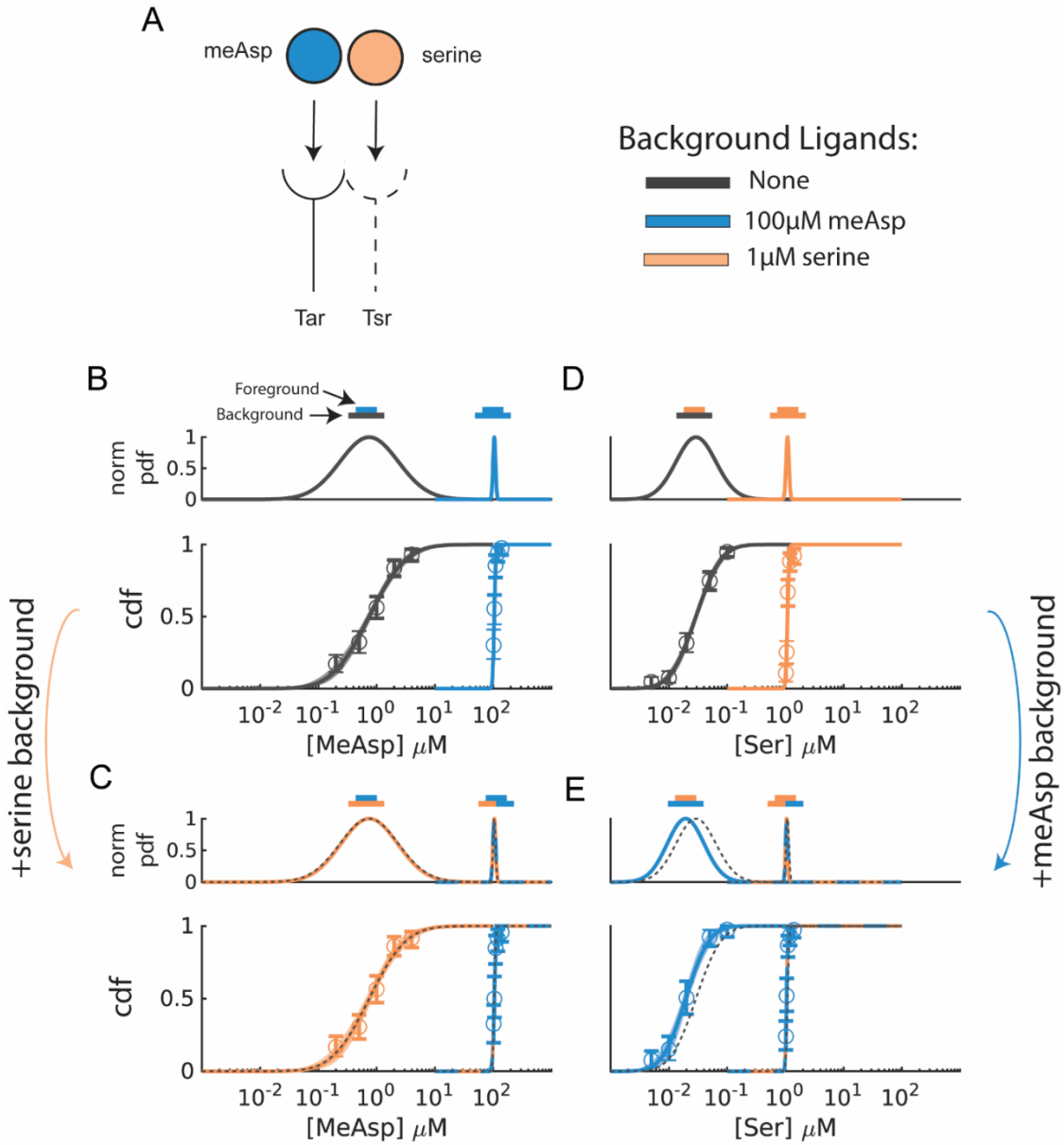

Figure 2. Responses to ligands that bind different receptors have independent $K_{1/2}$ distributions. A) We measured responses to meAsp and serine while varying the background concentration of both ligands. **B)** With no background ligands present, the meAsp $K_{1/2}$ is broadly distributed. After adaptation to 100uM meAsp however, it narrows ($n_{cells} =$ 153, 83, respectively for each curve left to right). Measured cdf with log-normal fit is shown on the bottom, while the normalized pdf is included above as a guide for the eyes. Curve colors correspond to the background condition. Double bar cartoons are included above each pdf to indicate the combination of foreground and background ligand in each curve. Shaded area around cdf curves are 95% confidence intervals. **C)** Adaptation to a 1uM serine background has no effect on the meAsp $K_{1/2}$ distribution with or without 100uM meAsp in the background ($n_{cells} = 108, 46$). Dotted line is the curve from panel B reproduced for comparison. **D)** Serine $K_{1/2}$ distribution before and after adaptation to a 1uM serine background ($n_{cells} = 174,\ 103$). **E)** Serine $K_{1/2}$ distributions after adaptation to 100 uM meAsp ($n_{cells} = 79, 75$). Dotted lines are curves from panel D, reproduced for comparison.

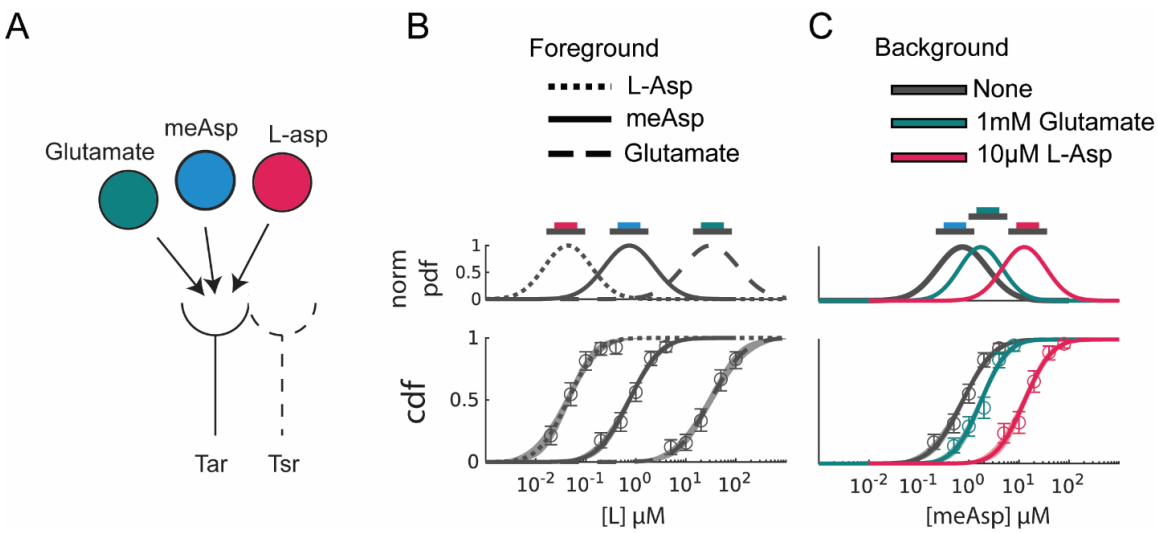

Figure 3. Competitive background ligands affect each other's mean sensitivity, but do not reduce $K_{1/2}$ diversity. A) We measured the $K_{1/2}$ distribution for 3 ligands that bind Tar with no background, and the $K_{1/2}$ distribution for meAsp in the presence of glutamate and L-asp. **B)** $K_{1/2}$ distributions for L-asp, meAsp and glutamate ($n_{cells} = 108, 158, 117$). While each distribution has a different mean corresponding to each ligands affinity for Tar, they all have similar CV. **C)** The meAsp $K_{1/2}$ distribution in the presence of glutamate or L-asp ($n_{cells} = 158, 127, 115$). In the presence of competitive background ligands, the mean $K_{1/2}$ shifts due to competition for binding sites, but the CV remains similar to the no-background case.

$K_{1/2}$ distribution for each ligand alone in plain motility medium. Surprisingly, even though the three ligands bind Tar with different affinities, their $K_{1/2}$ distributions had similar CVs (Figure 3B).

We then measured the meAsp $K_{1/2}$ distribution with either 1mM glutamate, or $10\mu M$ L-Asp in the background which both led to a noticeable shift in the mean meAsp $K_{1/2}$ (Figure 3C). The presence of these background ligands shifted the meAsp $K_{1/2}$ distribution to the right due to competition for receptor binding sites, but did not significantly impact the CV (Figure 3C,D; Figure S3). It appears that adaptation to ligands that binds the same receptor but are different from the foreground ligand (here meAsp) has no effect on the degree of $K_{1/2}$ diversity for the foreground ligand. This is true irrespective of the affinity of the background ligand. This behavior is surprising because it is in stark contrast to what happens when the identity of the background is the same as that of the foreground (Figure 2B).

$K_{1/2}$ diversity tuning is enabled by precise adaptation and competitive ligand binding.

How is it that the $K_{1/2}$ distribution of sensitivity to meAsp, which is mediated by the Tar receptor, behaves differently depending on whether meAsp or L-Asp is present in the background?

We sought to explain our results using a simple MWC modeling framework for chemoreceptor clusters (Keymer et al., 2006; Mello and Tu, 2005; Phillips, 2020; Tu, 2013). In this model, receptors are assumed to operate in an all-or-none fashion in strongly cooperative clusters that synchronously transition between kinase activating 'on' and kinase deactivating 'off' states (Figure 4A). The free energy difference between these two states is determined by the concentration of all ligands in the environment and the methylation level of the receptors. Due to precise adaptation (Barkai and Leibler, 1997; Yi et al., 2000), the change in free energy due to methylation always compensates for any changes in ligand concentration, ensuring that at steady state the system returns to the same total free energy.

Previously, by fitting the MWC model to the meAsp $K_{1/2}$ distribution in different backgrounds, we showed that $K_{1/2}$ variation was best explained by variation in the degree of receptor coupling, n (Kamino et al., 2020). However, there was no model for a direct prediction of the $K_{1/2}$ CV as a function of background ligand concentration. Motivated by our measurements, we derived an expression for the $K_{1/2}$ CV for a ligand L as a function of its background concentration L_0, and the concentration of all other competitive ligands (Figure 4B, Supplementary Appendix):

$$CV_L(L_0, C) = \frac{\sigma_0}{K_0 + L_0\left(1 + \frac{L_0}{K_i} + C\right)^{-1}} \tag{1}$$

where σ_0 and K_0 are the standard deviation and mean $K_{1/2}$ if no ligands are present, and C is the sum of all competing ligand concentrations scaled by their dissociation constants. This result crucially depends on the assumption that the system adapts precisely (Supplementary Appendix).

This model makes several quantitative predictions. First, it predicts the background concentration $L_0^{(1/2)}$ where the CV is exactly between its minimum and maximum values to be

$$L_0^{(1/2)} = \frac{K_0(1 + C)}{1 + K_0/K_i} \tag{2}$$

The $L_0^{(1/2)}$ is interesting quantity because at this ligand concentration, the coefficient of variation is $\frac{1}{2}(\frac{\sigma_0}{K_0} + \frac{\sigma_0}{K_0+K_i})$, which does not depend on L_0 or C, and as such does not change in the presence of a background signal unknown to the experimenter. For this reason, comparing the theoretical prediction and actual measurement of the CV at $L_0^{(1/2)}$can be used to diagnose whether measurements are done at a true zero-background condition.

With K_0 and σ_0 as free parameters, we were able to fit all the meAsp $K_{1/2}$ CVs measured in the absence of an L-asp background (Figure 4C) with good quantitative agreement. The fitted

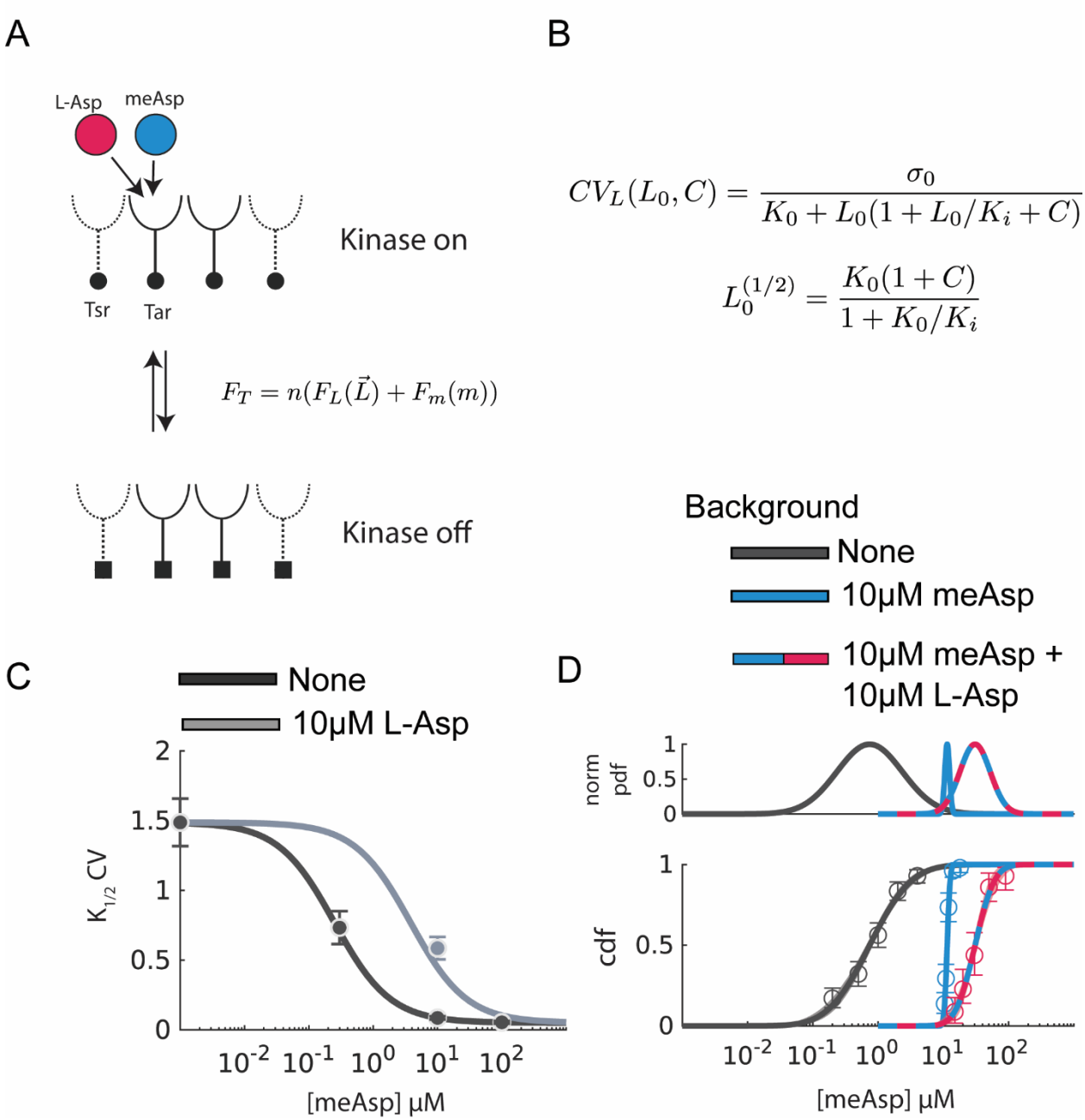

Figure 4. Mathematical model predicts that competitive ligands increase each other's $K_{1/2}$ diversity in non-zero backgrounds. A) The MWC model treats receptor clusters as a single unit with 'kinase on' and 'kinase off' states. The equilibrium activity is determined by the total free energy of the cluster F_T. **B)** This model allows prediction of the coefficient of variation (CV) in the $K_{1/2}$ for a ligand L given its background concentration L_0, and the effective concentration of all competing ligands, C. The transition from high to low diversity should occur when $L_0 = L_0^{(1/2)}$. **C)** The model (lines) was fit to measurements of the CV at 0, 10, and 100uM meAsp with no other ligands present. Position of $L_0^{(1/2)}$ was predicted to be ~0.3μM, and the CV in the presence of a 10 μM meAsp + 10 μM L-asp background was predicted, which were subsequently verified with experiments. Points are measured CVs with 95CI as error bars. **D)** Adaptation to 10 μM meAsp decreases the meAsp $K_{1/2}$ CV. Addition of 10 μM L-asp to the environments leads to an increase in $K_{1/2}$ diversity as predicted by the model ($n_{cells} = 158, 102, 57$).

K_0 and σ_0 were smaller than the experimental values from our zero-background condition indicating the presence of an unknown background signal that competes with meAsp.

We tested the predictive power of the model in a $10\mu M$ meAsp + $10\mu M$ L-asp background, which should lead to a dramatic increase in the CV compared to an experiment with only $10\mu M$ meAsp in the background. Our experiments aligned well with the prediction using no additional free parameters (Figure 4D). We concluded that the fitted model is a good quantitative predictor of the $K_{1/2}$ diversity given a particular background signal, which allows us to determine for a given ligand and mixed background signal, where the transition from the high-diversity to low-diversity regimes occurs.

Diverse sensitivities could improve navigation in complex chemical landscapes:

Our theory predicts how the $K_{1/2}$ CV shifts in response to changing background conditions. But does this transition have any functional consequences for populations of chemotactic bacteria? To see how the $K_{1/2}$ diversity collapse affects navigation, consider navigation in an exponential attractant gradient (Figure 5A). In such a gradient, the rate of change in log ligand concentration is constant in space. At the bottom of the gradient, sensitivity to movement up the gradient is diverse. For a fixed movement size, only a small fraction of the population will have a $K_{1/2}$ small enough to sense the change in ligand concentration. However, at the top of the gradient, all cells have similar sensitivity to the gradient for the same motion, such that as long as the gradient is sufficiently steep, all cells are able to sense it (Figure 5B).

We interpret this difference in the behavioral diversity at the bottom and top of the gradient as a transition from a bet-hedging to a tracking strategy. When a population first encounters a new gradient, they only commit a small fraction of the population to tracking it. However, a population higher on the gradient will commit more individuals, until nearly all cells are tracking the gradient. How do other nearby gradients affect this transition from one behavioral strategy to another? Uncompetitive ligand gradients will have no effect. Competitive gradients on the other hand, affect the fraction of the population able to sense the bottom of the gradient, but have virtually no effect as populations climb higher (Figure 5C).

To illustrate these effects, we used agent-based simulations of bacteria in an environment with two static, gaussian attractant peaks, where cells were challenged to locate the peak of either attractant (Figure 5D-F; Figure S4; Supplementary Appendix). We compared the performance of two populations: one where the degree of receptor coupling (n_{Tar} for Tar-associated ligands and n_{Tsr} for Tsr-associated ligands) varies (the diverse population), and one where each cell has the median n values of the first population (the uniform population). Cells were allowed to adapt to the ligand concentration at the origin, then after 1500s, cells of each population within 40um of either attractant peak were counted. At each peak, the relative performance was defined as the ratio of cells from the diverse population and cells from the uniform population at that peak.

From our argument above, we expect that the diverse and uniform populations behave similarly as the background increases. To illustrate this effect, we varied the concentration of serine

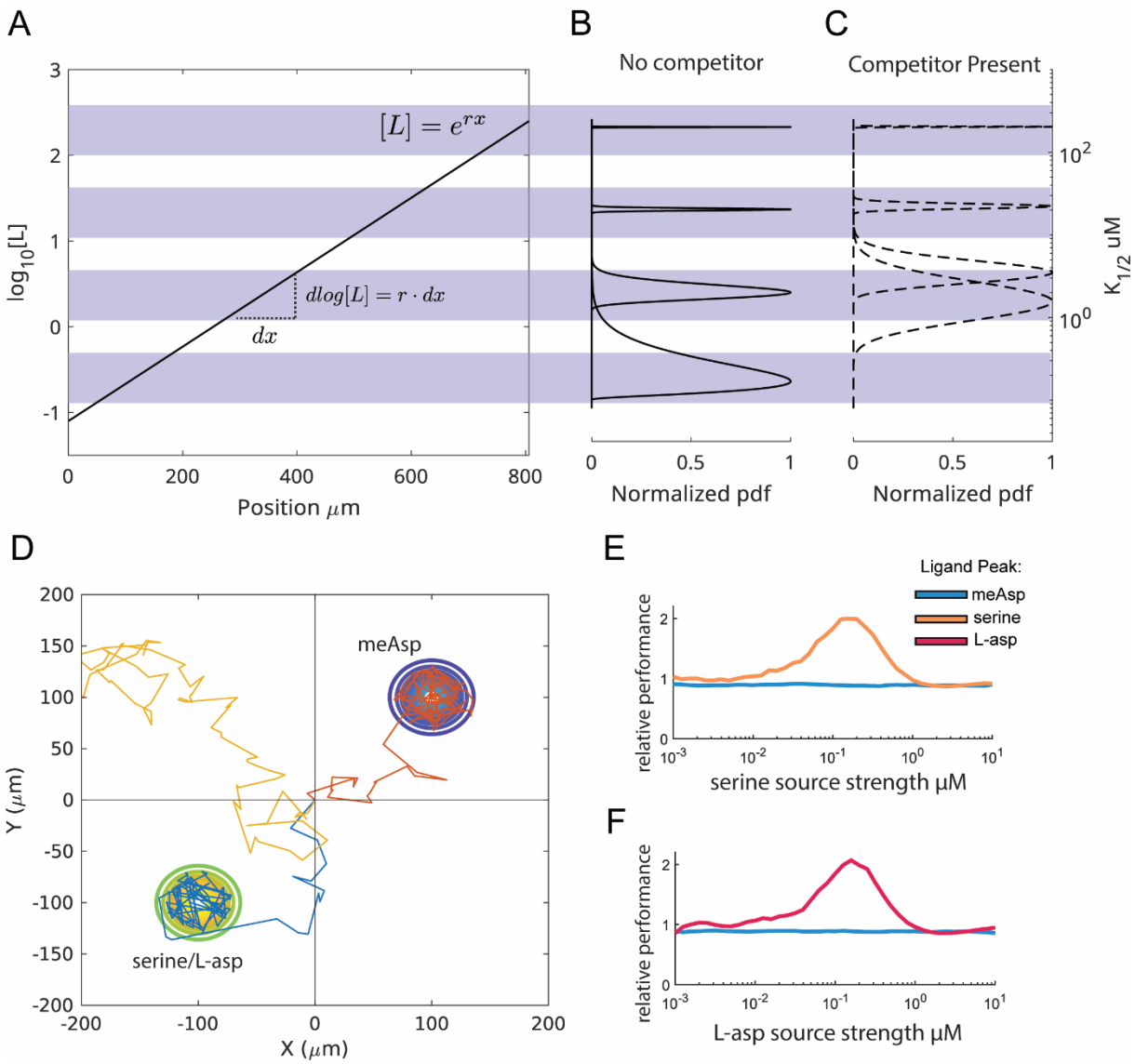

Figure 5: Interpretation of $K_{1/2}$ diversity as gradient sensitivity. **A)** During motion in an exponential gradient, the change in the log ligand concentration is constant. The $K_{1/2}$ distribution can be used to determine which cells are able to sense the gradient. **B)** For a gradient with exponential slope r, a motion dx in the gradient produces a signal $r \cdot dx$. At the bottom of the gradient, not all cells can sense this signal. However, at the top of the gradient, all cells are in the sensitive region (shaded). **C)** The presence of a competitor (non-zero value of C) changes how many cells are in the sensitive region at the bottom of the gradient. However, at the top, the distribution of sensitivities is unchanged. **D)** Agent-based simulation environment with static gaussian meAsp signal (blue), and serine or L-asp signal (green). Three example trajectories are shown. Cells were considered successful if they were within 40um of a source after 1500s. **E)** Relative performance of a population with diverse n values to a population with the median n value ($n_{cells} = 10{,}000$) at the meAsp peak with concentration fixed to 100uM, and variable serine peak concentration. Performance at the meAsp peak is not affected by varying the serine peak concentration, but at intermediate serine concentrations, the diverse population has up to a 2-fold advantage. **F)** Same simulation as in panel E, but with L-asp instead of serine. Even though both sources compete, at intermediate L-asp concentration, the diverse population has up to a 2-fold advantage.

at the serine peak, while leaving the meAsp peak at 100uM, and measured relative performance at each peak. As expected, at high serine peak concentration, the performance of the diverse and uniform populations is similar. However, at low to intermediate concentrations, the diverse population can have up to a 2-fold advantage (Figure 5E). Additionally, increasing performance at the serine peak did not compromise the population's ability to locate the meAsp peak.

Next, we asked how relative performance is affected when both attractant peaks compete for binding on the same receptor by replacing the serine peak with aspartate (Figure S4E-H). Consistent with our theory, the diverse and uniform populations perform similarly when the aspartate peak concentration is high. Interestingly however, the relative performance at the aspartate peak followed the same pattern as the serine peak, and did not compromise the population's ability to locate the meAsp peak (Figure 5F). Ultimately, our simulations suggest that the collapse of the $K_{1/2}$ distribution at high absolute ligand concentration allows populations to benefit from rare high sensitivity cells at the bottom of an attractant gradient, without compromising performance at the top of a gradient because of rare low-sensitivity cells.

Diversity tuning in other adaptive signaling architectures:

The bacterial chemosensory network is a classic example of negative integral feedback. However, other network architectures are also known to implement precise adaptation (Adler and Alon, 2018; Ferrell, 2016). The other most common class of networks with this property are incoherent feed-forward loops (Figure 6) where the input activates (deactivates) both the output and a repressor (activator) of the output. We asked whether adaptive feed-forward signaling networks tune sensory diversity as background conditions change.

We considered several variations on the type-1 incoherent feed-forward loop (Adler and Alon, 2018; Bintu et al., 2005; Ferrell, 2016; Goentoro et al., 2009; Shoval et al., 2010). We assumed the repressor y was always operating in the linear regime with respect to the input(s) x, and also rescaled the system of equations by the degradation and maximal activation rates of the output z. We found three configurations of the feed-forward loop that displayed diversity tuning similar to *E. coli*'s chemotaxis network. Diversity tuning was achieved by either (1) varying the concentration of second negative regulator of the output (Figure 6A), (2) having the input x bind a ligand with variable dissociation constant (Figure 6B), (3) or having a second input that behaves identically to the first input, with variable concentration (Figure 6C). The possible networks with this behavior is likely not limited to these cases, but these three illustrate how diversity tuning can be achieved through several mechanisms. In cases 1 and 3, diversity tuning arises because the effect of the second competitive regulator becomes negligible as the background input concentration increases. In the second case, diversity tuning arises because the system transitions to a fold-change sensing regime as the receptor nears total unsaturation.

Interestingly, in these feed-forward systems, not all parameters can have their variation tuned out at high input backgrounds. For example, in all three cases, varying the dissociation constants for x and y on z (K_x, K_y) results in $K_{1/2}$ diversity that is preserved at all background concentrations (Figure S5). This is a key difference with the MWC model for chemotaxis, where

variation in any of the model parameters will lead to $K_{1/2}$ diversity that decreases with increasing background ligand concentration.

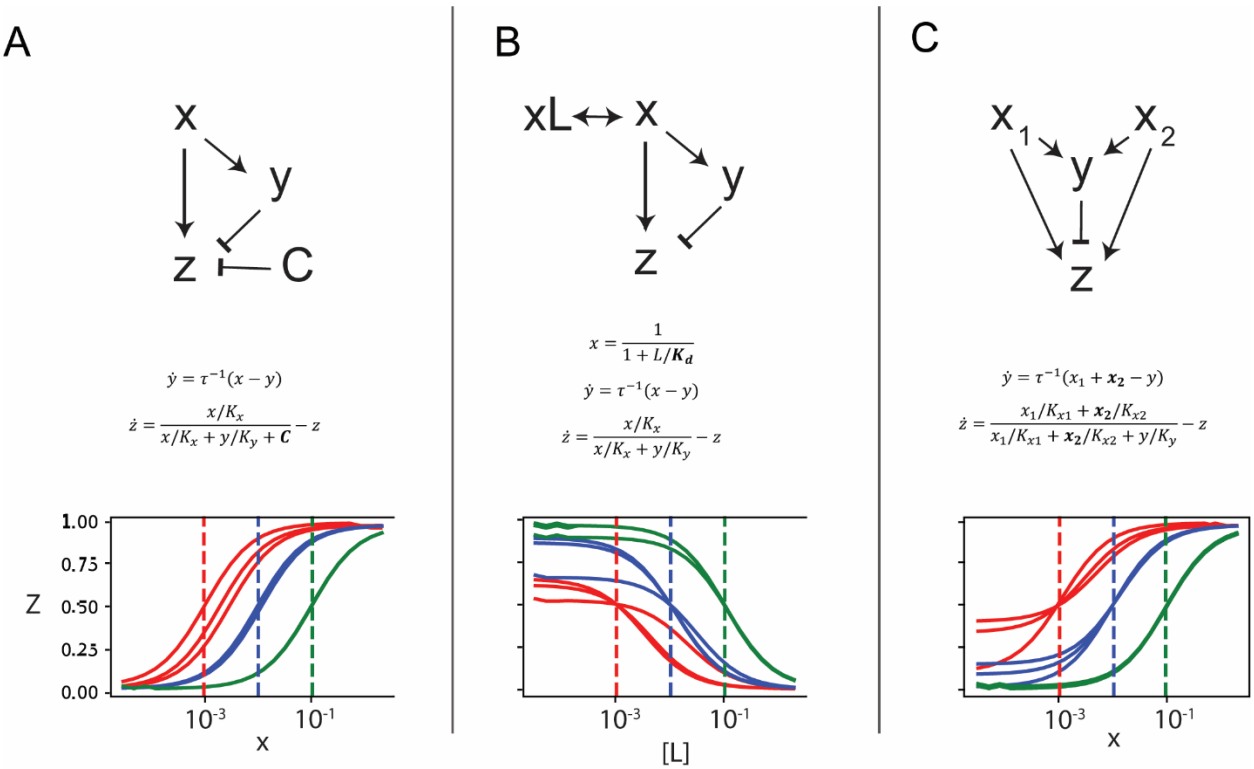

Figure 6: Diversity tuning in different incoherent feed-forward systems. Diversity tuning with increasing background concentration can be introduced to a type-1 incoherent feed-forward loop by introducing a new parameter in one of several ways. **A)** A competitive negative regulator (C) of the output independent of the core feed-forward loop, **B)** a ligand binding step that controls the input concentration, or **C)** a second feed forward system that competes with the first at each step. For each system, variation in the bolded parameter is tuned out by increasing the background input concentration, while the coefficient of variation in all other parameters (such as the dissociation constants for x and y) are unaffected. Dose response curves of several choices for the bold parameter are shown, with the background levels indicated by the dotted line.

Discussion:

Due to its extensive molecular and functional characterization, *E. coli* chemotaxis is an excellent testing ground for general principles of signal processing by living systems, and the role of cell-to-cell variation in population-level sensory strategies. In this study, we used single-cell FRET to measure the distribution of $K_{1/2}$ (sensitivity) for several ligands in various backgrounds. Consistent with previous work (Kamino et al., 2020), increasing the concentration of a particular ligand led to a decrease in the $K_{1/2}$ diversity for that ligand. In this work, we found that the $K_{1/2}$

diversity for two ligands that bind different receptors can be independently tuned. However, for ligands that bind the same receptor, increasing the background concentration of one ligand decreases $K_{1/2}$ diversity for that ligand, while increasing the diversity for its competitors.

An intuitive way to understand why the $K_{1/2}$ CV changes with background ligand concentration is to consider one of the unique features of the chemotaxis network: the transition from linear sensing to fold-change detection (Adler and Alon, 2018; Keymer et al., 2006; Lazova et al., 2011). When background ligands are low, cells respond to the absolute ligand concentration and the $K_{1/2}$ is highly sensitive to the degree of receptor coupling (Keymer et al., 2006). However, as the background concentration increases, cells transition to the fold-change detection regime where they respond to the relative change in ligand concentration. What do background ligands do to this transition? Uncompetitive ligands do not interfere with each other, whereas competitive ligands make the transition more difficult, but do not prevent collapse of the $K_{1/2}$ distribution. Our mathematical model of the $K_{1/2}$ CV allows us to quantitatively predict where the transition from the high to low diversity regimes occurs given an arbitrary mixture of background ligands.

An important aspect of this model is that the maximal degree of cell-to-cell variability for each ligand is independent of all background ligands, even those that bind the same receptor, where the mean sensitivity but not the CV changes. This invariance is enabled by precise adaptation to the background. While it is still possible to see the CV decrease with imprecise adaptation, in this case, adaptation to one ligand will affect the $K_{1/2}$ distribution of other ligands. Precise adaptation has been shown to be important in the context of single-cell navigation for climbing attractant gradients (Neumann et al., 2014; Wong-Ng et al., 2016). Our current findings reveal its importance in at the level of population-level navigation performance, by permitting populations to implement a bet-hedging strategy for multiple ligands independently at the same time.

Diversity tuning in response to environmental signals has been shown previously in metabolic pathways, including nitrogen fixation in *Klebsiella oxytoca* (Schreiber et al., 2016) and anaerobic respiration in *E. coli* (Carey and Goulian, 2019; Carey et al., 2018; Roggiani and Goulian, 2015). However, the general features leading to this behavior remain mysterious. The expression we derive for the diversity as a function of background ligand concentration is not specific to chemotaxis as we found similar expressions for the sensitivity CV for three feed-forward architectures (Supplementary appendix). Further exploration of our model is needed to reveal the relative importance of fold-change detection, precise adaptation, and network architecture in producing a response with diversity tuning.

Functionally, how might diversity in sensitivity ($K_{1/2}$) and the ability to tune this diversity in different backgrounds benefit bacterial populations? Behavioral studies previously revealed diversity in the chemotactic gain, and suggested that maintaining poor navigators in a population can protect the population from catastrophic events (Salek et al., 2019). Additionally, within each cell, temporal fluctuations in gain have been theorized to improve resource exploitation in complex environments by preventing cells from getting trapped in local attractant maxima (Karin and Alon, 2021). One implementation of pathway gain diversity which is consistent with our model, may be

variation in receptor coupling n, which has been suggested by previous work in ours and other labs (Kamino et al., 2020; Salek et al., 2019).

Our findings add important context to these previous results. Collapse of the $K_{1/2}$ distribution after adaptation to large ligand backgrounds suggest that variability in receptor cooperativity is only relevant to behavior when tracking signals with low absolute concentration. This is also supported by our agent-based simulations where we challenged cells to locate the center of a Gaussian ligand profile with varying source strength. When the source is weak, a diverse population has higher performance since rare high-gain cells can track the gradient. However, at high source strength, due to diversity tuning, the low-gain cells do not hamper performance, and behavior is similar to that of the median phenotype.

Ultimately, our data suggest that *E. coli* bacteria have evolved to implement sensory diversity in a way that allows the population to simultaneously use a bet-hedging strategy, where only some individuals will track new signals that appear, and a tracking strategy, where the population commits to climbing a particular signal gradient. This feature of the chemosensory receptor cluster could aid populations in making behavioral decisions. If weak signals appear, a small segment of the population will track them without committing the entire population to a potentially transient signal. Due to precise adaptation and the independence of the sensory diversity for different ligands, this behavioral strategy can be applied independently to different signals by the same population, at the same time. Our mathematical analysis of diversity tuning in simple incoherent feed-forward systems shows that background-dependent transitions between different bet-hedging regimes can arise in multiple non-trivial ways. As such, it would be interesting to measure cell-to-cell variability in the sensitivity of signaling or gene expression pathways controlled by incoherent feed-forward loops (Adler and Alon, 2018; Bintu et al., 2005; Ferrell, 2016; Goentoro et al., 2009; Tyson et al., 2003), where diversity tuning could be used to mitigate the effects of responding to transient signals.

Acknowledgements: We thank JS Parkinson and V. Sourjik for providing strains, and we thank F. Avgidis, D. Clark, N. Dimitrova, and H. Mattingly for useful discussions. **Funding:** This work was supported by NIH Awards R01GM106189 and R01GM138533. J.M. was supported by the NSF Graduate Research Fellowship Program under Grant No. DGE-2139841.

Author contributions: J.M., K.K. T.E., and T.S.S. designed the project. K.K. designed the experimental setup. J.M. and R.K. performed the experiments. J.M. performed the data analysis and mathematical modeling. J.M., K.K., T.E. and T.S.S. wrote the manuscript with input from R.K.

Declaration of Interests: The authors declare no competing interests. **Data and materials availability:** All data needed to evaluate the conclusions in the paper are present in the paper and/or the Supplementary Materials. Additional data may be requested from the authors.

Methods:

Strains and Plasmids:

All FRET experiments were performed with a derivative of *E. coli* K-12 RP437 (HCB33). The FRET donor (CheY-mRFP) and acceptor (CheZ-mYFP) were expressed in tandem on the plasmid pSJAB106 (Keegstra et al., 2017) from an isopropyl-β-d-thiogalactopyranoside (IPTG)–inducible promoter with 50 uM IPTG. To adhere cells to glass coverslips, a glass-adhesive mutant of FliC (FliC*) was expressed from a sodium salycilate (NaSal)-inducible promoter on the plasmid pZR1 (Keegstra, 2017) with 3 uM NaSal. Plasmids were transformed in a *cheY, cheZ, fliC* triple deletant in a previous publication (Kamino et al., 2020).

Microfluidics Fabrication and operation:

Microfluidic devices were constructed from PDMS with standard soft lithography methods (Qin et al., 2010). The master mold for the device was a silicon wafer with features created using ultraviolet photoresist lithography (Figure S1). To cast the device, the mold was coated with a 5 mm-thick layer of degassed 10:1 PDMS-to-curing agent mixture (Sylgard 184, Dow Chemical). Molds were baked at 80°C for 45 min. Devices were cut out of the mold and holes were punched into the inlets with a manually sharpened 20-guage blunt-tip needle. Then, PDMS devices were bonded to a 24mm X 60mm coverslip (#1.5). PDMS was cleaned with transparent adhesive tape (Magic tape, Scotch) then rinsed with acetone, isopropanol, methanol, and water. Coverslips were also rinsed with acetone, isopropanol, methanol, and water. Glass and PDMS were treated with plasma generated by a corona treater. Then, PDMS was laminated to the coverslip, and baked overnight at 80°C.

The microfluidic device has 7 inlets, an outlet at the end of the imaging chamber, and two side outlets of which only the right one is opened during cell loading (Figure S1). During operation, the inlets were connected to 7 reservoirs containing motility media and various stimuli. Cells washed in motility medium were loaded into the device through the outlet channel, where they initially exit through one of the side outlets, which is plugged before imaging to induce flow towards the end outlet. Pressure in the inlet reservoirs was controlled by computer-controlled solenoid valves (MH1, Festo) that quickly switch between atmospheric pressure, and a source of pressurized air as needed.

In vivo single-cell FRET microscopy:

Single-cell FRET and cell culture were performed as previously (Kamino et al., 2020). Cells were diluted from an overnight culture into 10mL fresh tryptone broth (1% bacto-tryptone, 0.5% NaCl) and grown to an OD between 0.44 and 0.46 in the presence of 100ug/mL ampicillin, 34ug/mL chloramphenicol, 50uM IPTG, and 3uM NaSal. Cells were centrifuged and washed twice with motility media (10mM KPO4, 0.1mM EDTA, 1uM methionine, 10mM lactic acid) then suspended in 2mL of motility media and left at room temperature for 2hrs before imaging.

FRET imaging was performed with an inverted microscope (Eclipse Ti-E, Nikon) equipped with an oil immersion objective (CFI Apo TIRF 60X Oil, Nikon). Yellow fluorescent proteins were illuminated with a light-emitting diode system (SOLA SE, Lumencore) through one excitation filter (59026x, Chroma), then another (FF01-550/24-25, Semrock) and a dichroic mirror (F01-542/27-25F, Semrock). Emission was fed into an emission image splitter (OptoSplit II, Cairn) where it was split into donor and acceptor channels with a dichroic mirror (FF580-FDi01-25x36, Semrock) and collected through emission bandpass filters (FF520-Di02-25x36 and FF593-Di03-25x36, Semrock) with a scientific CMOS camera (ORCA-Flask4.0 V2, Hammatsu). Red fluorescent protein was imaged in the same was as YFP, except with a different second excitation filter (FF01-575/05-25) and dichroic mirror (FF593-Di03-25x36, Semrock). Images were collected with 50ms exposure.

FRET data analysis:

Single-cell fluorescent signals were extracted from fluorescence time-series as described previously (Kamino et al., 2020; Keegstra et al., 2017; Zal and Gascoigne, 2004). Images were segmented and single-cell fluorescent signals determined with in-house software. Time-series were corrected for photobleaching by fitting donor and acceptor time-series with a bi-exponential function and dividing out the decay to yield donor $D(t)$ and acceptor $A(t)$ signals.

To calculate FRET from fluorescence time-series, we used the E-FRET method (Zal and Gascoigne, 2004). The E-FRET index is given by

$$FRET = E_{app} = \frac{I_{DA} - aI_{AA} - dI_{DD}}{I_{DA} - aI_{AA} + (G - d)I_{DD}}$$

where I_{DA} is FRET-acceptor emission intensity from donor excitation, I_{AA} is acceptor emission with acceptor excitation, I_{DD} is donor emission from donor excitation, with a, G, d being optical constants that depend on the FRET pair and optical setup (Zal and Gascoigne, 2004) which were determined by an independent experiment with strains that express only CheY-mRFP or only CheZ-mYFP (Mattingly et al., 2021).

To convert FRET time-series to kinase activity, for each cell, FRET values were normalized by the minimum and maximum values measured during a saturating stimulus at the beginning and end of the experiment. For each experiment, the saturating stimulus was a mixture of the background stimulus, and a saturating amount of the foreground stimulus.

Determining $K_{1/2}$ distribution from single-cell responses:

We utilized the method described in (Kamino et al., 2020) to determine the $K_{1/2}$ cumulative distribution from single-cell responses to multiple stimulus levels. Given a family of dose-response curves, for a given ligand concentration $[L]_i$, the fraction of responses that are greater than half-maximal equals the fraction of cells with $K_{1/2} < [L]_i$ (Figure S1). Thus, by determining the

fraction of half-maximal responses at a series of ligand concentrations, we can measure the cumulative distribution function (CDF) of the $K_{1/2}$. For each measured point on the CDF, confidence intervals were determined by bootstrapping, both over cells and over the seven responses per re-sampled cell. Confidence intervals (95% CI) on the fitted lognormal parameters were estimated from the posterior distribution with lognormal priors and gaussian error using markov-chain monte carlo methods (Figure S2).

Behavioral simulations:

Agent-based simulations (SI Appendix) were run using in-house software adapted from previous studies (Dufour et al., 2016; Frankel et al., 2014; Long et al., 2017). Briefly, the standard model of *E. coli* chemotaxis (Keymer et al., 2006; Mello and Tu, 2005; Tu, 2013; Tu et al., 2008) was integrated using Euler's method. The model was extended to include cell-to-cell variation in receptor coupling for two receptor species. Receptors are described by a two-state model where activity is determined by the free energy difference between the active and inactive states which is itself determined by the ligand concentration and receptor methylation level. At each time-step, the cell moves forward or remains in place depending on its motility state (run/tumble), each with a characteristic rotational diffusion. At the new position, the ligand concentration is updated, and the methylation level adjusted. The updated free energy of the receptor cluster determines the switching rate between run and tumble.

References:

Adler, M., and Alon, U. (2018). Fold-change detection in biological systems. Current Opinion in Systems Biology *8*, 81-89.

Barkai, N., and Leibler, S. (1997). Robustness in simple biochemical networks. Nature *387*, 913-917.

Bintu, L., Buchler, N.E., Garcia, H.G., Gerland, U., Hwa, T., Kondev, J., and Phillips, R. (2005). Transcriptional regulation by the numbers: models. Current Opinion in Genetics & Development *15*, 116-124.

Burt, A., Cassidy, C.K., Ames, P., Bacia-Verloop, M., Baulard, M., Huard, K., Luthey-Schulten, Z., Desfosses, A., Stansfeld, P.J., Margolin, W.*, et al.* (2020). Complete structure of the chemosensory array core signalling unit in an E. coli minicell strain. Nature Communications *11*.

Carey, J.N., and Goulian, M. (2019). A bacterial signaling system regulates noise to enable bet hedging. Current Genetics *65*, 65-70.

Carey, J.N., Mettert, E.L., Roggiani, M., Myers, K.S., Kiley, P.J., and Goulian, M. (2018). Regulated Stochasticity in a Bacterial Signaling Network Permits Tolerance to a Rapid Environmental Change. Cell *173*, 196-207.e114.

Colin, R., Rosazza, C., Vaknin, A., and Sourjik, V. (2017). Multiple sources of slow activity fluctuations in a bacterial chemosensory network. Elife *6*.

Dufour, Y.S., Gillet, S., Frankel, N.W., Weibel, D.B., and Emonet, T. (2016). Direct Correlation between Motile Behavior and Protein Abundance in Single Cells. PLoS Comput Biol *12*, e1005041.

Ferrell, J.E. (2016). Perfect and Near-Perfect Adaptation in Cell Signaling. Cell Systems *2*, 62-67.

Frank, V., Piñas, G.E., Cohen, H., Parkinson, J.S., and Vaknin, A. (2016). Networked Chemoreceptors Benefit Bacterial Chemotaxis Performance. mBio *7*, e01824-01816.

Frankel, N.W., Pontius, W., Dufour, Y.S., Long, J., Hernandez-Nunez, L., and Emonet, T. (2014). Adaptability of non-genetic diversity in bacterial chemotaxis. Elife *3*.
Goentoro, L., Shoval, O., Kirschner, M.W., and Alon, U. (2009). The Incoherent Feedforward Loop Can Provide Fold-Change Detection in Gene Regulation. Mol Cell *36*, 894-899.
Hallem, E.A., and Carlson, J.R. (2006). Coding of Odors by a Receptor Repertoire. Cell *125*, 143-160.
Hurley, A., and Bassler, B.L. (2017). Asymmetric regulation of quorum-sensing receptors drives autoinducer-specific gene expression programs in Vibrio cholerae. PLOS Genetics *13*, e1006826.
Kadakia, N., and Emonet, T. (2019). Front-end Weber-Fechner gain control enhances the fidelity of combinatorial odor coding. eLife *8*.
Kamino, K., Keegstra, J.M., Long, J., Emonet, T., and Shimizu, T.S. (2020). Adaptive tuning of cell sensory diversity without changes in gene expression. Science Advances *6*, eabc1087.
Karin, O., and Alon, U. (2021). Temporal fluctuations in chemotaxis gain implement a simulated-tempering strategy for efficient navigation in complex environments. iScience *24*, 102796.
Keegstra, J.M., Kamino, K., Anquez, F., Lazova, M.D., Emonet, T., and Shimizu, T.S. (2017). Phenotypic diversity and temporal variability in a bacterial signaling network revealed by single-cell FRET. Elife *6*.
Keymer, J.E., Endres, R.G., Skoge, M., Meir, Y., and Wingreen, N.S. (2006). Chemosensing in Escherichia coli: Two regimes of two-state receptors. Proceedings of the National Academy of Sciences *103*, 1786-1791.
Korobkova, E., Emonet, T., Vilar, J.M., Shimizu, T.S., and Cluzel, P. (2004). From molecular noise to behavioural variability in a single bacterium. Nature *428*, 574-578.
Lan, G., Schulmeister, S., Sourjik, V., and Tu, Y. (2011). Adapt locally and act globally: strategy to maintain high chemoreceptor sensitivity in complex environments. Mol Syst Biol *7*, 475.
Lazova, M.D., Ahmed, T., Bellomo, D., Stocker, R., and Shimizu, T.S. (2011). Response rescaling in bacterial chemotaxis. Proc Natl Acad Sci U S A *108*, 13870-13875.
Long, J., Zucker, S.W., and Emonet, T. (2017). Feedback between motion and sensation provides nonlinear boost in run-and-tumble navigation. PLOS Computational Biology *13*, e1005429.
Mattingly, H.H., Kamino, K., Machta, B.B., and Emonet, T. (2021). Escherichia coli chemotaxis is information limited. Nat Phys.
Mello, B.A., and Tu, Y. (2005). An allosteric model for heterogeneous receptor complexes: Understanding bacterial chemotaxis responses to multiple stimuli. Proceedings of the National Academy of Sciences *102*, 17354-17359.
Narla, A.V., Borenstein, D.B., and Wingreen, N.S. (2021). A biophysical limit for quorum sensing in biofilms. Proceedings of the National Academy of Sciences *118*, e2022818118.
Neumann, S., Hansen, C.H., Wingreen, N.S., and Sourjik, V. (2010). Differences in signalling by directly and indirectly binding ligands in bacterial chemotaxis. The EMBO journal *29*, 3484-3495.
Neumann, S., Vladimirov, N., Krembel, A.K., Wingreen, N.S., and Sourjik, V. (2014). Imprecision of adaptation in Escherichia coli chemotaxis. PLoS One *9*, e84904.
Park, H., Pontius, W., Guet, C.C., Marko, J.F., Emonet, T., and Cluzel, P. (2010). Interdependence of behavioural variability and response to small stimuli in bacteria. Nature *468*, 819-823.
Parkinson, J.S., Hazelbauer, G.L., and Falke, J.J. (2015). Signaling and sensory adaptation in Escherichia coli chemoreceptors: 2015 update. Trends in microbiology *23*, 257-266.
Pfister, P., Smith, B.C., Evans, B.J., Brann, J.H., Trimmer, C., Sheikh, M., Arroyave, R., Reddy, G., Jeong, H.-Y., Raps, D.A*., et al.* (2020). Odorant Receptor Inhibition Is Fundamental to Odor Encoding. Current Biology *30*, 2574-2587.e2576.
Phillips, R. (2020). The molecular switch : signaling and allostery, 1. edn (Princeton: Princeton University Press).
Piñas, G.E., Frank, V., Vaknin, A., and Parkinson, J.S. (2016). The source of high signal cooperativity in bacterial chemosensory arrays. Proceedings of the National Academy of Sciences *113*, 3335-3340.

Qin, D., Xia, Y., and Whitesides, G.M. (2010). Soft lithography for micro- and nanoscale patterning. Nature Protocols *5*, 491-502.
Qin, S., Li, Q., Tang, C., and Tu, Y. (2019). Optimal compressed sensing strategies for an array of nonlinear olfactory receptor neurons with and without spontaneous activity. Proceedings of the National Academy of Sciences *116*, 20286-20295.
Roggiani, M., and Goulian, M. (2015). Oxygen-Dependent Cell-to-Cell Variability in the Output of the Escherichia coli Tor Phosphorelay. Journal of Bacteriology *197*, 1976-1987.
Salek, M.M., Carrara, F., Fernandez, V., Guasto, J.S., and Stocker, R. (2019). Bacterial chemotaxis in a microfluidic T-maze reveals strong phenotypic heterogeneity in chemotactic sensitivity. Nature Communications *10*.
Schreiber, F., Littmann, S., Lavik, G., Escrig, S., Meibom, A., Kuypers, M.M.M., and Ackermann, M. (2016). Phenotypic heterogeneity driven by nutrient limitation promotes growth in fluctuating environments. Nature Microbiology *1*, 16055.
Shoval, O., Goentoro, L., Hart, Y., Mayo, A., Sontag, E., and Alon, U. (2010). Fold-change detection and scalar symmetry of sensory input fields. Proc Natl Acad Sci U S A *107*, 15995-16000.
Sourjik, V., and Berg, H.C. (2002). Receptor sensitivity in bacterial chemotaxis. *99*, 123-127.
Sourjik, V., and Berg, H.C. (2004). Functional interactions between receptors in bacterial chemotaxis. Nature *428*, 437-441.
Tu, Y. (2013). Quantitative modeling of bacterial chemotaxis: signal amplification and accurate adaptation. Annu Rev Biophys *42*, 337-359.
Tu, Y., Shimizu, T.S., and Berg, H.C. (2008). Modeling the chemotactic response of Escherichia coli to time-varying stimuli. Proceedings of the National Academy of Sciences *105*, 14855-14860.
Tyson, J.J., Chen, K.C., and Novak, B. (2003). Sniffers, buzzers, toggles and blinkers: dynamics of regulatory and signaling pathways in the cell. Current Opinion in Cell Biology *15*, 221-231.
Wong-Ng, J., Melbinger, A., Celani, A., and Vergassola, M. (2016). The Role of Adaptation in Bacterial Speed Races. PLoS Comput Biol *12*, e1004974.
Yang, Y., M. Pollard, A., Höfler, C., Poschet, G., Wirtz, M., Hell, R., and Sourjik, V. (2015). Relation between chemotaxis and consumption of amino acids in bacteria. Molecular Microbiology *96*, 1272-1282.
Yi, T.M., Huang, Y., Simon, M.I., and Doyle, J. (2000). Robust perfect adaptation in bacterial chemotaxis through integral feedback control. P Natl Acad Sci USA *97*, 4649-4653.
Zal, T., and Gascoigne, N.R. (2004). Photobleaching-corrected FRET efficiency imaging of live cells. Biophys J *86*, 3923-3939.

Supplemental Appendix:

Model of the chemotaxis pathway:

We used the standard model of bacterial chemotaxis (Keymer *et al.*, 2006; Mello and Tu, 2005; Phillips, 2020; Tu, 2013; Tu *et al.*, 2008) where the cell relays sensory information to the flagellar motor through a signaling cascade triggered by binding of attractant to highly cooperative receptor arrays. Receptor clusters whose activity can be described by a two-state model where activity $a \in [0,1]$ is determined by the free energy difference F (in units of $k_B T$) between the active and inactive states

$$a = \frac{1}{1 + e^F}$$

The free energy can be decomposed into two terms $F = F_m(m) + F_{\vec{L}}(\vec{L})$. The first depends linearly on the degree of receptor methylation m, such that $F_m(m) = -n_T \alpha (m - m_0)$ where n_T is the total receptor coupling, and α and m_0 are constants (Shimizu et al., 2010). The second term is the dependence of the free energy on ligand binding, where $\vec{L}$ is a vector containing the concentrations of all ligand species in the environment. The form of $F_L(L)$ will depend on whether the ligands bind competitively or uncompetitively to the receptor cluster. For two ligands that bind either Tar or Tsr but not both,

$$F_{\vec{L}}(\vec{L}) = n_{tar} \ln\left(\frac{1 + \frac{L_1}{K_{i,1}}}{1 + \frac{L_1}{K_{a,1}}}\right) + n_{tsr} \ln\left(\frac{1 + \frac{L_2}{K_{i,2}}}{1 + \frac{L_2}{K_{a.2}}}\right)$$

where n_{Tar} and n_{Tsr} are the receptor coupling of Tar and Tsr respectively, L_1 and L_2 are concentrations of ligands binding Tar and Tsr respectively with dissociation constants K_i and K_a to the inactive and active receptor states. In the case where L_1 and L_2 both bind Tar in the same binding pocket,

$$F_{\vec{L}}(\vec{L}) = n_{tar} \ln\left(\frac{1 + \frac{L_1}{K_{i,1}} + \frac{L_2}{K_{i,2}}}{1 + \frac{L_1}{K_{a,1}} + \frac{L_2}{K_{a,2}}}\right)$$

As the external ligand concentration changes, receptors are methylated or demethylated to adapt to maintain an activity level a_0 independent of the environment. To describe methylation kinetics, we used a similar approach as previous studies, where

$$\frac{dm}{dt} = V_R \cdot \frac{1 - a}{K_R + 1 - a} - V_B(a) \cdot \frac{a}{K_B + a}$$

where V_R and $V_B(a) = V_B(0)\left(1 + \theta(\mathrm{a} - \mathrm{a_B})\frac{a - a_B}{1 - a_B} r_B\right)$ (θ is the Heaviside function and $a_B = 0.74, r_B = 4.0$) are the methylation/demethylation rates for CheR and CheB with dissociation constants, K_R and K_B.

We assume signal transduction to be fast compared to methylation, so that the active response regulator CheY-P concentration can bet written, $Y(a) = \alpha a$ with α constant. CheY-P binds the flagellar motor, changing the switching rate between clockwise (CW) and counter-clockwise (CCW) rotation. This switching is assumed to be a Poisson process with switching rates

$$\lambda_{CCW \to CW}(Y) = \omega e^{-G(Y)}$$
$$\lambda_{CW \to CCW}(Y) = \omega e^{G(Y)}$$

where $G(Y) = \frac{\epsilon_1}{4} + \frac{\epsilon_2}{2}\frac{1}{1+K/Y}$ with $\epsilon_1, \epsilon_2, K$ constant (Frankel *et al.*, 2014; Long *et al.*, 2017; Sneddon *et al.*, 2012). We assume that only a single motor switching from $CCW \rightarrow CW$ is sufficient to tumble, so for cells with only 1 flagellum, the rates above describe the run and tumble dynamics as a function of CheY-P.

Agent-based simulations:

Agent-based simulations were performed using Euler integration of the above model, as described previously (Dufour *et al.*, 2014; Frankel *et al.*, 2014; Long *et al.*, 2017; Sneddon *et al.*, 2012). At each time-step, the cell either moves or stays in place depending on its motility state (run or tumble), which both have their own rotational diffusion coefficients D_R and D_T. After updating the position and local ligand concentration, the adaptation equation is integrated and the free energy of the receptors, and thus the CheY-P concentration and motor switching rates are updated. A random number is drawn to determine whether the flagellum state switches, with rules and parameters as in (Sneddon *et al.*, 2012).

Cells were challenged to navigate an environment with two static gaussian gradients, given by $L(x) = L_0 e^{-r(\vec{x}-\overrightarrow{x_0})^2}$, where L_0 is the ligand concentration at the starting position, $\overrightarrow{x_0}$ is the center of the gaussian, and r is the gradient ramp rate. The gradients were placed equidistant from the origin where cells were initialized. Additionally, for each cell, values of n_{tar} and n_{tsr} were drawn by sampling from the experimental $K_{1/2}$ distribution for meAsp in 0-background, and using the conversion $n \approx K_{\frac{1}{2}} \cdot \log(2)/K_i$. For simplicity, the same distribution was assumed for both n_{Tar} and n_{Tsr}. To isolate the effect of signal integration and diversity in receptor coupling, we assumed that methylation does not saturate, which would lead to imperfect adaptation as the population climbs the gradient (Neumann *et al.*, 2014; Wong-Ng *et al.*, 2016).

Quantitative model of the $K_{1/2}$ CV as a function of background ligands:

To determine the coefficient of variation (CV) of the $K_{1/2}$, we utilized the classic MWC model of bacterial chemoreceptor clusters, as above. For a ligand L, assuming $L \ll K_a$, the activity of the cluster is approximately

$$a(L, \epsilon) \approx \left[1 + \left(1 + \frac{L}{K_i} + C\right)^n Ue^{\epsilon}\right]^{-1}$$

where ϵ is the free energy of the cluster in the absence of all ligands, $C = \sum_l L_l/K_l$ is a constant that accounts for the presence of all background attractants that compete with L, and U is a constant that accounts for all uncompetitive ligands.

We assume that the receptor cluster adapts perfectly. This means that at steady state, any combination of ligands will result in the same activity, given by

$$a_0 = [1 + e^{\epsilon_0}]^{-1}$$

where ϵ_0 is the adapted zero-background free energy. Now, we can define the $K_{1/2}$ as the ligand concentration L where $a(L, \epsilon) = a_0/2$. We also write $L = L_0 + \Delta L$ where L_0 is the background concentration of L. To find the $K_{1/2}$, we solve

$$a(L,\epsilon) = \frac{a_0}{2}$$

$$\left[1 + \left(1 + \frac{L}{K_i} + C\right)^n U e^{\epsilon}\right]^{-1} = \frac{1}{2}[1+\epsilon_0]^{-1}$$

$$\left[1 + \left(1 + \frac{L_0}{K_i} + \frac{\Delta L}{K_i} + C\right)^n U e^{\epsilon}\right]^{-1} = \frac{1}{2}[1+\epsilon_0]^{-1}$$

$$\left[1 + \left(1 + \frac{\Delta L}{K_i^{eff}}\right)^n e^{\epsilon^{eff}}\right]^{-1} = \frac{1}{2}[1+\epsilon_0]^{-1}$$

where $K_i^{eff} = K_i\left(1 + \frac{L_0}{K_i} + C\right)$ and $\epsilon^{eff} = \epsilon + \ln(U) + n \cdot \ln(1+C) = \epsilon_0$ due to perfect adaptation. Continuing,

$$\left[1 + \left(1 + \frac{\Delta L}{K_i^{eff}}\right)^n e^{\epsilon_0}\right]^{-1} = \frac{1}{2}[1+\epsilon_0]^{-1}$$

$$1 + \left(1 + \frac{\Delta L}{K_i^{eff}}\right)^n e^{\epsilon_0} = 2 + 2e^{\epsilon_0}$$

$$\Delta L = K_i^{eff}[(e^{-\epsilon_0} + 2)^{\frac{1}{n}} - 1]$$

Thus, the $K_{1/2}$ as defined above, is given by $K_{1/2} = \left(1 + \frac{L_0}{K_i} + C\right) K_i \left[(e^{-\epsilon_0} + 2)^{\frac{1}{n}} - 1\right] + L_0$.

The $K_{1/2}$ clearly depends on both the free energy of the the cluster in zero background ϵ_0, and the degree of receptor coupling, n. We assume that the receptor-ligand affinity K_i and background ligand experienced L_0 is the same for each cell. Thus, we can write the average $K_{1/2}$ as

$$\left\langle K_{\frac{1}{2}} \right\rangle = \left(1 + \frac{L_0}{K_i} + C\right) \left\langle K_i \left[(e^{-\epsilon_0} + 2)^{\frac{1}{n}} - 1\right] \right\rangle + L_0 = \left(1 + \frac{L_0}{K_i} + C\right) K_0 + L_0$$

and the standard deviation as

$$SD\left(K_{\frac{1}{2}}\right) = \left(1 + \frac{L_0}{K_i} + C\right) SD\left(K_i \left[(e^{-\epsilon_0} + 2)^{\frac{1}{n}} - 1\right]\right) = \left(1 + \frac{L_0}{K_i} + C\right) \sigma_0$$

Then, the coefficient of variation (CV) in $K_{1/2}$ is given by

$$CV = \frac{\sigma_0}{K_0 + L_0/(1 + \frac{L_0}{K_i} + C)}$$

By inspection, the maximal CV is σ_0/K_0, and the minimal CV is $\sigma_0/(K_0 + K_i)$. Given a particular competitive background C, the transition between the high and low diversity regimes occurs when

$$L_0 = L_0^{\left(\frac{1}{2}\right)} = \frac{K_0(1+C)}{1 + K_0/K_i}$$

Remark on the effects of imprecise adaptation:

A critical step in the derivation above is to assume that at steady state, the effect free energy of the cluster $\epsilon_{eff} = \epsilon_0$ no matter the background concentration. If this is not the case, then K_0 and σ_0 are no longer constants, and cannot be interpreted as the average and standard deviation of the true zero-background $K_{1/2}$ since they will be sensitive to the background. How K_0 and σ_0 are affected by a background-dependent ϵ_0 will depend on the microscopic details of the system, and as such cannot be accounted for by our model.

Diversity tuning in the incoherent feed-forward architecture:

To explore the generality of diversity tuning in adaptive signaling networks, we examined how background signals affect sensitivity of another common signaling architecture: the incoherent feed-forward loop. In general, these systems are described by a system of differential equations:

$$\dot{y} = \tau^{-1}(x - y)$$

$$\dot{z} = G(x, y) - z$$

where we have assumed that the y dynamics are in the linear regime, and rescaled time by the degradation rate of z. By assuming different forms of $G(x, y)$ we can derive similar expressions to equation 1 in the main text. We considered three such functions which correspond to different perturbations of the basic feed-forward loop (Figure 6; Figure S5): (1) the presence of a third species who represses z and varies independently from the three feed-forward loop species (Figure 6a); (2) a conversion of x between active and inactive conformations based on ligand occupancy (Figure 6b); and lastly, (3) a parallel feed-forward system that competes for binding sites with x at each stage (Figure 6c). The following result is very similar for all three cases, so we only include the full argument for the first case.

Let $G(x, y) = \frac{\frac{x}{K_x}}{\frac{x}{K_x} + \frac{y}{K_y} + C}$. Here, x activates z, while y and some other regulator C inhibit z. If we assume the y dynamics are slow compared to z ($\tau \gg 1$) we can calculate the dose-response curve with respect to the input x. As a function of the current x value,

$$z(x) = \frac{x}{x + K_x\left(\frac{x_{ss}}{K_y} + C\right)}$$

This has a minimum value of 0, and a maximum value of 1. For simplicity, we'll define the $K_{1/2}$ as the value of x where $z(x) = \frac{1}{2}$, but the argument works out similarly if we define the $K_{1/2}$ midway between the steady state value and the minimum or maximum values. The $K_{1/2}$ is easily recognized as

$$K_{1/2} = \frac{K_x}{K_y} x_{ss} + K_x C$$

If we allow C but not K_x or K_y to vary, we find that

$$\left\langle K_{\frac{1}{2}} \right\rangle = \frac{K_x}{K_y} x_{ss} + K_x \langle C \rangle = \frac{K_x}{K_y} x_{ss} + K_0$$

$$SD\left(K_{\frac{1}{2}}\right) = K_x SD(C) = \sigma_0$$

$$CV = \frac{\sigma_0}{\frac{K_x}{K_y} x_{ss} + K_0}$$

Where K_0 is the $K_{1/2}$ when $x_{ss} = 0$, and σ_0 is the standard deviation of $K_{1/2}$ when $x_{ss} = 0$. As with chemotaxis, the $K_{1/2}$ diversity for this incoherent feed-forward loop decreases sigmoidaly with the background concentration. A key difference however, is that here, the CV decreases to 0 as $x_{ss} \to \infty$, whereas in chemotaxis, there is a non-zero limiting CV. Additionally, unlike chemotaxis where none of the parameters are multiplied by the background, for this feed-forward loop, K_x and K_y are scaled by the background. As such, if they are varied, the resulting $K_{1/2}$ variation is not reduced as the background increases (Figure S5).

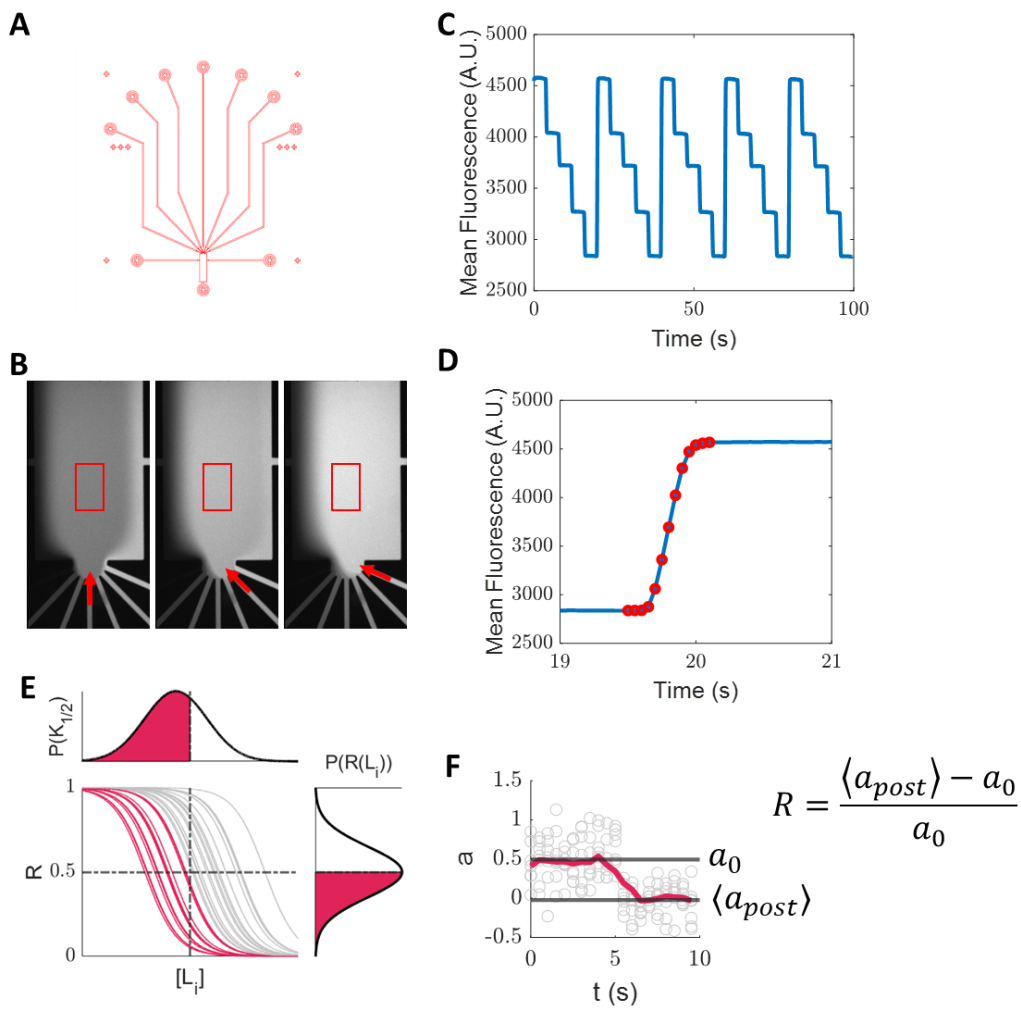

Figure S1: Seven-inlet microfluidic device developed to measure sensitivity distributions. **A)** Design of the device, which has seven inlets (top), two side outlets, and one main outlet (bottom). Before an experiment, cells are introduced through the main outlet, where they circle through the main chambre, and exit through one of the side outlets. The other side outlet is unused. **B)** Image of the main chamber with the approximate field of view boxed in red. The stimulus concentration of the pressurized channel (red arrow) fully covers the field of view. **C)** Switching between channels filled with different fluoresceine concentrations over time. **D)** To fully turn over the solution in the device takes approximately 0.2 seconds. Each dot is the average fluorescence of the field of view for one frame, with images taken at 20fps. **E)** Use of the device to determine $K_{1/2}$ distribution. The cumulative distribution function of the $K_{1/2}$ can be calculated from single-cell responses to multiple stimulus levels. For a given stimulus level L_i, the probability that a cell's response amplitude is <0.5 equals the probability that the $K_{1/2}$ is less than L_i. **F)** Response amplitude in this context is defined as the fractional change in kinase activity during a stimulus. All seven responses were included to determine the average pre-stimulus activity, and average post-stimulus activity.

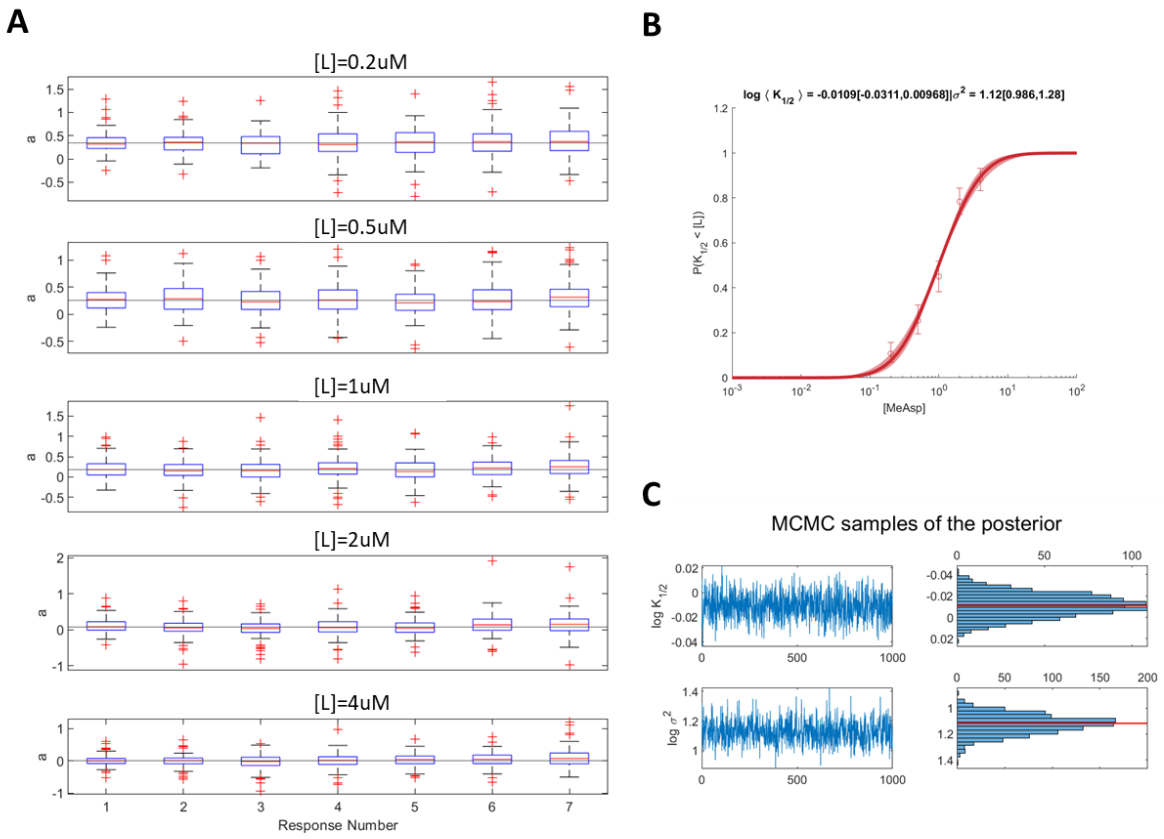

Figure S2: Stationarity of the response distribution and parameter estimation. **A)** Distribution of post-stimulus kinase activity for seven responses at five stimulus levels. There are not major shifts in the response distribution over the course of the experiment, a necessary condition for our method to estimate the K1/2 distribution. Parameters of the K1/2 cumulative distribution function **(B)** were determined by maximum likelihood fitting of lognormal parameters. Error bars on the data are 95-CI, calculated by bootstrapping over both the cells included in the analysis, and the seven responses used to calculate each cell's response amplitude. Uncertainty in the lognormal parameters was determined by sampling the posterior **(C)** with lognormal priors.

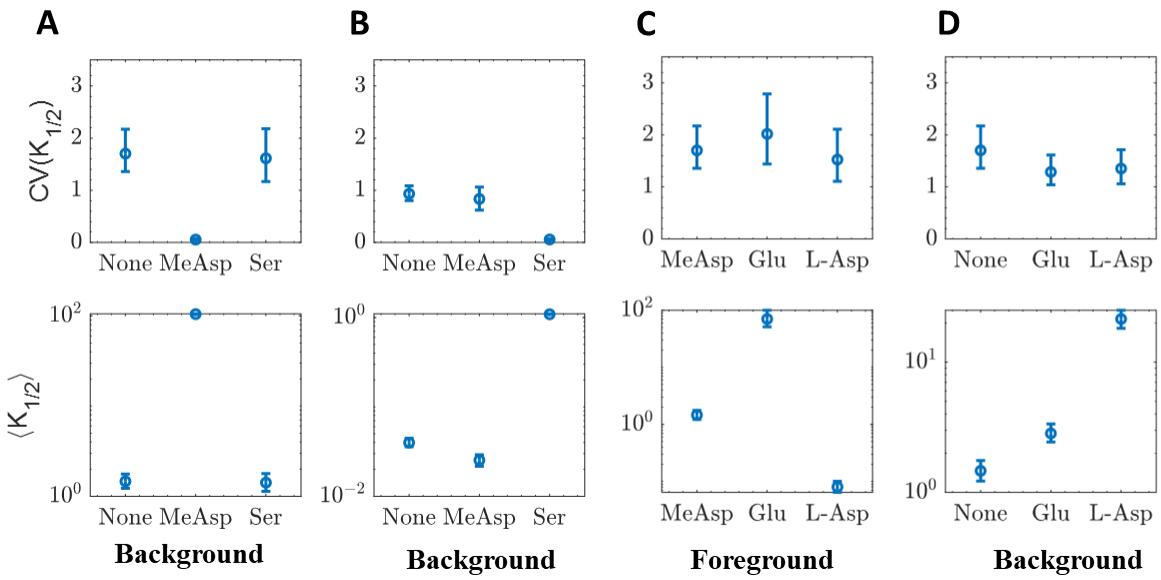

Figure S3: Statistical analysis of K1/2 distribution for the main figures. Plotted are the CV's and mean K1/2 for each measured K1/2 distribution in the main text. Dots are the median of values calculated from the Markov chain monte carlo (MCMC) samples of the CDF parameters, and error bars are the 95% confidence intervals. **A)** Data from Figure 2A: meAsp $K_{1/2}$ in plain motility medium, 100 uM meAsp, or 1uM serine. **B)** Data from Figure 2C: serine $K_{1/2}$ in plain motility medium, 100 uM meAsp, or 1uM serine. **C)** Data from Figure 3A: $K_{1/2}$ distributions for three foreground ligands in plain motility medium. **D)** Data from Figure 3C: $K_{1/2}$ distribution for meAsp in three background conditions: plain motility medium, 1mM glutamate, or 10 uM L-Asp.

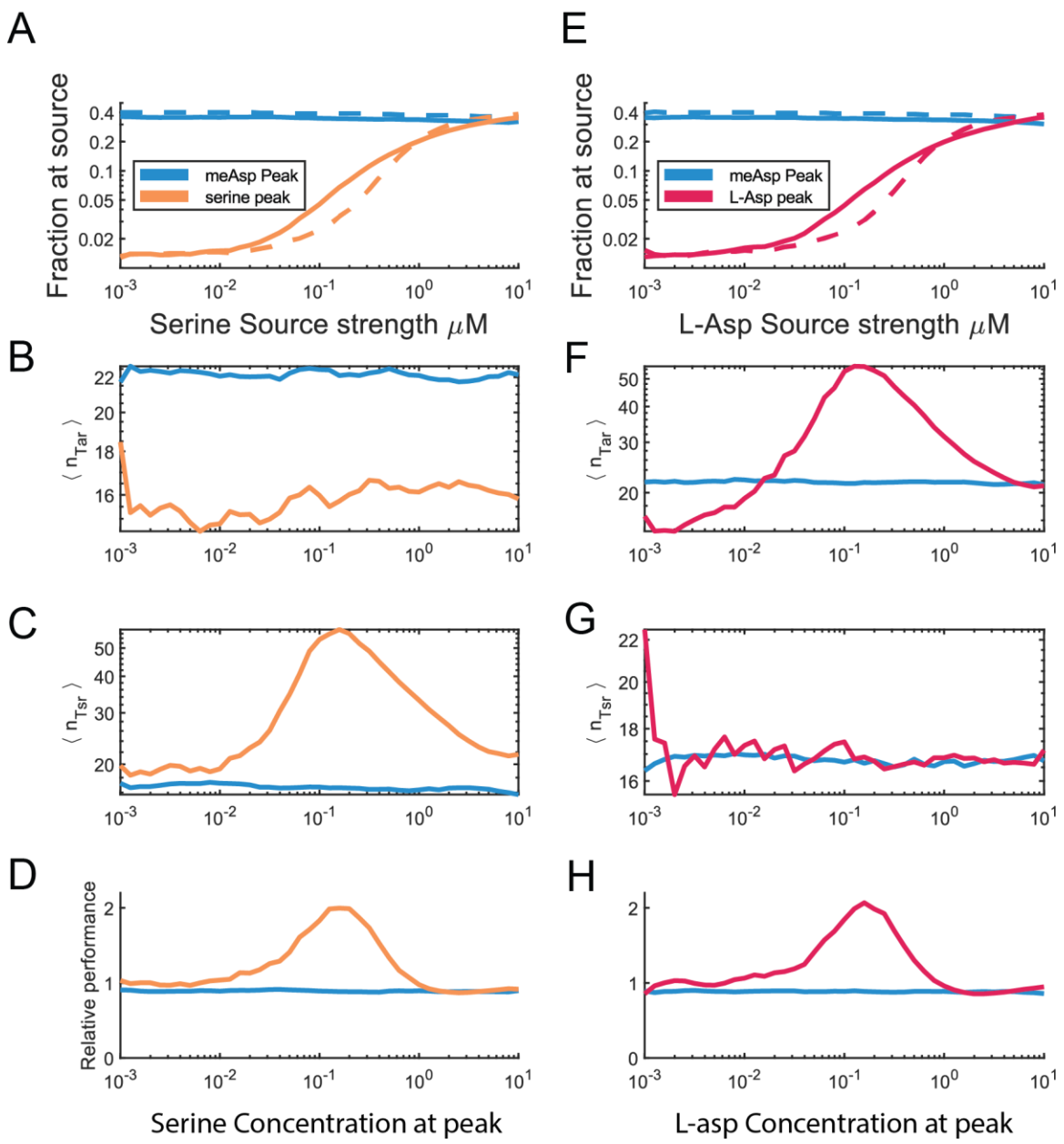

Figure S4: Behavioral simulations with sensitivity diversity. **A)** Accumulation at a serine or meAsp peak for a diverse population (solid line) and a population with uniform n_{Tar} and n_{Tsr} (dotted line), as described in main text. **B)** Median n_{Tar} at the meAsp peak and the serine peak. **C)** Median n_{Tsr} at the serine and meAsp peak. **D)** Relative performance of diverse population to the homogenous population at the serine and meAsp peaks. The diverse population gains up to a 2-fold advantage for intermediate concentrations of serine. **E-H)** Same measurements as A-D but with the serine peak replaced with an L-asp peak with the same statistics. Even with this competitive attractant peak, the diverse population has up to a 2-fold advantage of the homogenous population at intermediate L-asp source strength.

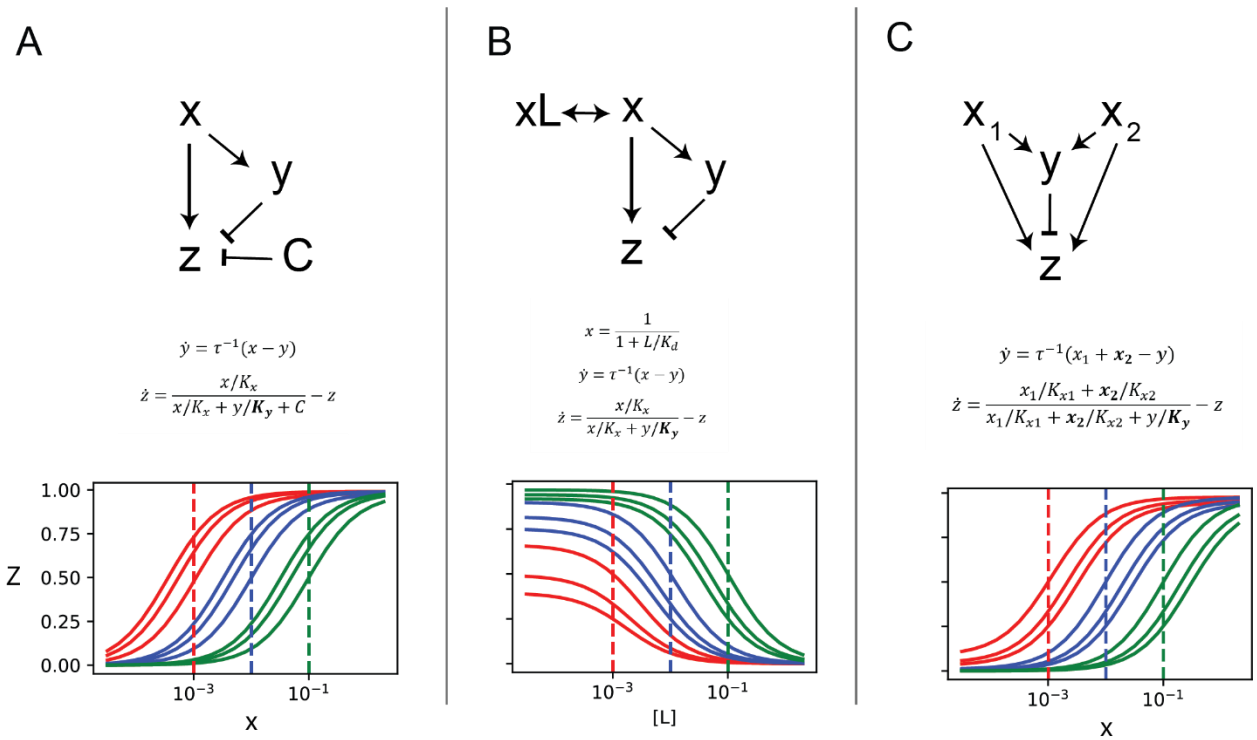

Figure S5: Variation in some parameters is not tuned by incoherent feed-forward loops. Here, we varied the dissociation constant of Y on Z for three configurations of the incoherent feed-forward loop, as in Figure 6. Variation in K_y results in dose-response curve diversity that remains similar no matter the background input concentration. This is in stark contrast to the case of bacterial chemotaxis, where variation in any parameters will be tuned out as the background signal increases.